Supplement of

Quantifying Drivers of Tropospheric OH and Its Trends: Sensitivity to Atmospheric Processes and Implications for Methane Lifetime

Xuewei Hou[1,2*], Ryan Hossaini[1*], Oliver Wild[1], Andrea Mazzeo[1], Richard J. Pope[3,4], Ye Wang[1], Siyuan Wang[5], Yuanhong Zhao[6], James Lee[7,8], Bin Zhu[2], Tianliang Zhao[2], Alok K. Pandey[9]

[1]Lancaster Environment Centre, Lancaster University, Lancaster, LA1 4YW, UK.

[2]Collaborative Innovation Center on Forecast and Evaluation of Meteorological Disasters, School of Atmospheric Physics, Nanjing University of Information Science and Technology, Nanjing, 210044, China.

[3]School of Earth and Environment, University of Leeds, Leeds, LS2 9JT, UK.

[4]National Centre for Earth Observation, University of Leeds, Leeds, LS2 9JT, UK.

[5]Department of Atmospheric Sciences, University of Miami, Florida, FL 33124, USA.

[6]State Key Laboratory of Physical Oceanography, Ocean University of China, Qingdao, 266100, China.

[7]Department of Chemistry, University of York, York, YO10 5DD, UK.

[8]National Centre for Atmospheric Science, University of York, York, YO10 5DD, UK.

[9]Department of Environmental Sciences, Deshbandhu College, University of Delhi, New Delhi, 110019, India.

Correspondence to: Xuewei Hou (x.hou4@lancaster.ac.uk) and Ryan Hossaini (r.hossaini@lancaster.ac.uk)

Table S1. Bimolecular gas-phase reactions included in the FRSGC/UCI CTM.

	Reactants	Products	A	E_a/R	Ref.
1	HO_2+HO_2	$\rightarrow H_2O_2+O_2$	3.00×10^{-13}	-460	[1]
2	HO_2+MeOO	$\rightarrow O_2+MeOOH$	4.10×10^{-13}	-750	[1]
3	HO_2+NO	$\rightarrow OH+NO_2$	3.44×10^{-12}	-260	[1]
4	HO_2+NO_3	$\rightarrow O_2+HONO_2$	1.75×10^{-12}	0	[1]
5	HO_2+NO_3	$\rightarrow OH+NO_2+O_2$	1.75×10^{-12}	0	[1]
6	HO_2+O_3	$\rightarrow OH+O_2+O_2$	1.00×10^{-14}	490	[1]
7	$MeOO+MeOO$	$\rightarrow 2HCHO+2HO_2+O_2$	9.50×10^{-14}	-390	[1]
8	$MeOO+NO$	$\rightarrow HCHO+NO_2+HO_2$	2.80×10^{-12}	-300	[1]
9	$N_2O_5+H_2O$	$\rightarrow HONO_2+HONO_2$	2.00×10^{-21}	0	[1]
10	$NO+NO_3$	$\rightarrow NO_2+NO_2$	1.70×10^{-11}	-125	[1]
11	$NO+O_3$	$\rightarrow NO_2+O_2$	3.00×10^{-12}	1500	[1]
12	NO_2+NO_3	$\rightarrow NO+NO_2+O_2$	4.35×10^{-14}	1335	[1]
13	NO_2+O_3	$\rightarrow NO_3+O_2$	1.20×10^{-13}	2450	[1]
14	NO_3+HCHO	$\rightarrow HONO_2+CO+HO_2$	5.80×10^{-16}	0	[1]
15	$O(^3P)+H_2O_2$	$\rightarrow OH+HO_2$	1.40×10^{-12}	2000	[1]
16	$O(^3P)+HCHO$	$\rightarrow OH+CO+HO_2$	3.40×10^{-11}	1600	[1]
17	$O(^3P)+HO_2$	$\rightarrow OH+O_2$	3.00×10^{-11}	-200	[1]
18	$O(^3P)+HO_2NO_2$	$\rightarrow$products	7.80×10^{-11}	3400	[1]
19	$O(^3P)+HONO_2$	$\rightarrow OH+NO_3$	3.00×10^{-17}	0	[1]
20	$O(^3P)+N_2O_5$	$\rightarrow$products	3.00×10^{-16}	0	[1]
21	$O(^3P)+NO_2$	$\rightarrow O_2+NO$	5.10×10^{-12}	-198	[2]
22	$O(^3P)+NO_3$	$\rightarrow O_2+NO_2$	1.30×10^{-11}	0	[1]
23	$O(^3P)+O_3$	$\rightarrow O_2+O_2$	8.00×10^{-12}	2060	[1]
24	$O(^3P)+OH$	$\rightarrow O_2+HO_2$	1.80×10^{-11}	-180	[1]
25	$O(^1D)+CH_4$	$\rightarrow OH+MeOO$	1.66×10^{-10}	0	[1]

26	$O(^1D)+CH_4$	$\rightarrow HCHO+H_2$	8.75×10^{-12}	0	[1]
27	$O(^1D)+H_2O$	$\rightarrow OH+OH$	1.63×10^{-10}	-60	[1]
28	$O(^1D)+N_2$	$\rightarrow O(^3P)+N_2$	2.15×10^{-11}	-110	[1]
29	$O(^1D)+O_2$	$\rightarrow O(^3P)+O_2$	3.3×10^{-11}	-55	[1]
30	$O(^1D)+O_3$	$\rightarrow O_2+O(^3P)+O(^3P)$	1.2×10^{-10}	0	[1]
31	$O(^1D)+O_3$	$\rightarrow O_2+O_2$	1.2×10^{-10}	0	[1]
32	$OH+CH_4$	$\rightarrow H_2O+MeOO$	2.45×10^{-12}	1775	[1]
33	OH+CO	$\rightarrow HO_2+CO_2$	1.5×10^{-13}	0	[4]
34	$OH+H_2$	$\rightarrow H_2O+HO_2$	2.8×10^{-12}	1800	[1]
35	$OH+H_2O_2$	$\rightarrow H_2O+HO_2$	1.8×10^{-12}	0	[1]
36	OH+HCHO	$\rightarrow H_2O+CO+HO_2$	5.5×10^{-12}	-120	[1]
37	$OH+HO_2$	$\rightarrow H_2O+O_2$	4.8×10^{-11}	-250	[1]
38	$OH+HO_2NO_2$	$\rightarrow H_2O+NO_2$	4.5×10^{-13}	-610	[1]
39	$OH+HONO_2$	$\rightarrow H_2O+NO_3$	1.5×10^{-13}	0	[3]
40	OH+MeOOH	$\rightarrow H_2O+HCHO+OH$	1.14×10^{-12}	-200	[1]
41	OH+MeOOH	$\rightarrow H_2O+MeOO$	2.66×10^{-12}	-200	[1]
42	$OH+NO_3$	$\rightarrow HO_2+NO_2$	2×10^{-11}	0	[1]
43	$OH+O_3$	$\rightarrow HO_2+O_2$	1.7×10^{-12}	940	[1]
44	OH+OH	$\rightarrow H_2O+O(^3P)$	1.8×10^{-12}	0	[1]
45	C_2H_6+OH	$\rightarrow EtOO$	7.66×10^{-12}	1020	[1]
46	EtOO+NO	$\rightarrow MeCHO+HO_2+NO_2$	2.6×10^{-12}	-365	[1]
47	EtOO+EtOO	$\rightarrow 2MeCHO+2HO_2$	6.8×10^{-14}	0	[1]
48	EtOO+MeOO	$\rightarrow MeCHO+HCHO+2HO_2$	2.5×10^{-14}	0	[4]
49	MeCHO+OH	$\rightarrow 0.5MeCO_3+0.5MeOO+0.5CO$	4.63×10^{-12}	-350	[1]
50	$MeCHO+NO_3$	$\rightarrow MeCO_3+HONO_2$	1.4×10^{-12}	1900	[1]
51	$MeCO_3+NO$	$\rightarrow MeOO+NO_2$	8×10^{-12}	-270	[1]
52	$MeOO+MeCO_3$	$\rightarrow HCHO+MeOO+HO_2$	2×10^{-12}	-500	[1]
53	$MeCO_3+MeCO_3$	$\rightarrow MeOO+MeOO$	2.9×10^{-12}	-500	[1]
54	PAN+OH	$\rightarrow HCHO+NO_2$	4×10^{-14}	0	[1]
55	$EtOO+HO_2$	$\rightarrow EtOOH$	7.5×10^{-13}	-700	[1]
56	EtOOH+OH	$\rightarrow EtOO+H_2O$	1.9×10^{-12}	-190	[5]
57	EtOOH+OH	$\rightarrow MeCHO+OH$	8.01×10^{-12}	0	[5]
58	Alkane+OH	$\rightarrow EtOO+MeOO+CO$	1.02×10^{-11}	430	[1]
59	$Alkene+O_3$	$\rightarrow HCHO+0.5MeCHO+CO$	6.5×10^{-15}	1900	[1]
60	ROHOO+NO	$\rightarrow HCHO+MeCHO+NO_2$	2.7×10^{-12}	-360	[5]
61	$ROHOO+HO_2$	$\rightarrow HCHO+MeCHO+OH$	1.53×10^{-13}	-1300	[5]
62	ROHOO+MeOO	$\rightarrow 2HCHO+MeCHO+HO_2$	1×10^{-13}	0	[5]
63	Aromatic+OH	$\rightarrow ArOO+HO_2$	1.8×10^{-12}	-340	[5]
64	ArOO+NO	$\rightarrow MeCO_3+4CO+NO_2$	4.2×10^{-12}	-360	[5]
65	$ArOO+HO_2$	$\rightarrow MeCO_3+4CO+OH$	1.5×10^{-13}	-1310	[5]
66	$Isoprene+O_3$	$\rightarrow MVKMACR+HCHO+OH$	1.1×10^{-14}	2000	[1]
67	Isoprene+OH	$\rightarrow IsopOO$	3×10^{-11}	-360	[1]
68	IsopOO+NO	$\rightarrow MVKMACR+HCHO+NO_2$	2.7×10^{-12}	-360	[5]
69	$IsopOO+HO_2$	$\rightarrow EtOOH+CO+CO$	2.05×10^{-13}	-1300	[5]
70	IsopOO+MeOO	$\rightarrow MVKMACR+2HCHO+2HO_2$	1×10^{-13}	0	[5]
71	$MVKMACR+O_3$	$\rightarrow 0.5MeCO_3+HCHO+MeOO$	8.5×10^{-16}	1520	[5]
72	MVKMACR+OH	$\rightarrow MVKOO$	2.6×10^{-12}	-610	[5]
73	MVKOO+NO	$\rightarrow 0.5MeCO_3+HCHO+NO_2$	2.7×10^{-12}	-360	[5]
74	$MVKOO+HO_2$	$\rightarrow EtOOH+CO$	1.82×10^{-13}	-1300	[5]
75	MVKOO+MeOO	$\rightarrow MeCO_3+2HCHO+HO_2$	1×10^{-13}	0	[5]

Note: T is the model grid-box temperature in Kelvin. $k=A\exp(-E_a/(RT))$. 1. Burkholder et al., 2020; 2. https://iupac.aeris-data.fr/catalogue/#/catalogue/classifications/gap, last access: 16 January 2026; 3. Atkinson et al., 2004; 4. Atkinson et al., 2006; 5. https://mcm.york.ac.uk/MCM/, last access: 16 January 2026.

Table S2. Termolecular gas-phase reactions included in the FRSGC/UCI CTM.

	Reactants	Products	f	k_1	α_1	β_1	k_2	α_2	β_2	Ref
1	HO_2+HO_2+M	$\rightarrow H_2O_2+O_2+M$	0.00	2.10×10^{-33}	0.00	-920.0	0.00	0.00	0.0	[1]
2	HO_2+NO_2+M	$\rightarrow HO_2NO_2+M$	0.60	1.90×10^{-31}	-3.40	0.0	6.00×10^{-12}	-0.30	0.0	[2]
3	HO_2NO_2+M	$\rightarrow HO_2+NO_2+M$	0.50	4.10×10^{-05}	0.00	10650.0	$5.70\times10^{+15}$	0.00	11170.0	[3]
4	N_2O_5+M	$\rightarrow NO_2+NO_3+M$	0.35	1.30×10^{-03}	-3.50	11000.0	$9.70\times10^{+14}$	0.10	11080.0	[4]
5	$NO+NO+M$	$\rightarrow NO_2+NO_2+M$	0.00	4.25×10^{-39}	0.00	-663.5	0.00	0.00	0.0	[4]
6	NO_2+NO_3+M	$\rightarrow N_2O_5+M$	0.60	2.40×10^{-30}	-3.00	0.0	1.60×10^{-12}	0.10	0.0	[1]
7	$O(^3P)+NO+M$	$\rightarrow NO_2+M$	0.60	9.10×10^{-32}	-1.50	0.0	3.00×10^{-11}	0.00	0.0	[1]
8	$O(^3P)+NO_2+M$	$\rightarrow NO_3+M$	0.60	1.30×10^{-31}	-1.50	0.0	2.30×10^{-11}	-0.24	0.0	[4]
9	$O(^3P)+O_2+M$	$\rightarrow O_3+M$	0.00	6.10×10^{-34}	-2.40	0.0	0.00	0.00	0.0	[1]
10	$O(^1D)+N_2+M$	$\rightarrow N_2O+M$	0.00	2.80×10^{-36}	-0.90	0.0	0.00	0.00	0.0	[1]
11	$OH+NO_2+M$	$\rightarrow HONO_2+M$	0.60	2.00×10^{-30}	-3.60	0.0	3.60×10^{-11}	0.00	0.0	[2,5]
12	$OH+OH+M$	$\rightarrow H_2O_2+M$	0.60	6.90×10^{-31}	-1.00	0.0	2.60×10^{-11}	0.00	0.0	[1]
13	$MeCO_3+NO_2+M$	$\rightarrow PAN+M$	0.30	3.28×10^{-28}	-6.87	0.0	1.13×10^{-11}	-1.11	0.0	[4]
14	$PAN+M$	$\rightarrow MeCO_3+NO_2+M$	0.30	1.10×10^{-05}	0.00	10100.0	$1.90\times10^{+17}$	0.00	14100.0	[4]
15	Alkene+OH+M	$\rightarrow ROHOO+M$	0.60	4.70×10^{-27}	-4.00	0.0	2.60×10^{-11}	-1.30	0.0	[1]

Note: T is the model grid-box temperature in Kelvin. 1. Burkholder et al., 2020; 2. Rolletter et al., 2025; 3. Atkinson et al., 2004; 4. https://iupac.aeris-data.fr/catalogue/#/catalogue/classifications/gap, last access: 18 March 2025; 5. Amedro et al., 2019.

$$k = \left(\frac{k_0[M]}{1+k_0[M]/k_\infty}\right) f^{\left(1+\left[log10\left(\frac{k_0[M]}{k_\infty}\right)\right]^2\right)^{-2}} \quad (1)$$

$$k_0 = k_1\left(\frac{T}{300}\right)^{\alpha_2}\exp\left(\frac{-\beta_1}{T}\right), \quad k_\infty = k_2\left(\frac{T}{300}\right)^{\alpha_2}\exp\left(\frac{-\beta_2}{T}\right) \quad (2)$$

Table S3. Photolysis reactions in the FRSGC/UCI CTM.

	Reactants	Products	Ratio(%)
1	$H_2O+h\nu$	$OH+HO_2$	0
2	$H_2O_2+h\nu$	2OH	100
3	$HCHO+h\nu$	$CO+H_2$	100
4	$HCHO+h\nu$	$CO+2HO_2$	100
5	$HO_2+h\nu$	$OH+O(^3P)$	0
6	$HO_2NO_2+h\nu$	$OH+NO_3$	33.3
7	$HO_2NO_2+h\nu$	HO_2+NO_2	66.7
8	$HONO_2+h\nu$	$OH+NO_2$	100
9	$MeOOH+h\nu$	$HCHO+OH+HO_2$	50
10	$MeOOH+h\nu$	$HCHO+O(^3P)+HO_2$	50
11	$N_2O_5+h\nu$	NO_3+NO_2	100
12	$NO_2+h\nu$	$NO+O(^3p)$	100
13	$NO_3+h\nu$	$NO+O_2$	100
14	$NO_3+h\nu$	$NO_2+O(^3P)$	100
15	$O_2+h\nu$	$2O(^3P)$	100
16	$O_3+h\nu$	$O_2+O(^3P)$	100
17	$O_3+h\nu$	$O_2+O(^1D)$	100
18	$MeCHO+h\nu$	$MeOO+HO_2+CO$	100
19	$MeCHO+h\nu$	CH_4+CO	100
20	$PAN+h\nu$	$MeCO_3+NO_2$	100

21	EtOOH+hν	MeCHO+HO_2+OH	100

Note: These photolysis reactions refer Wild et al. (2000)

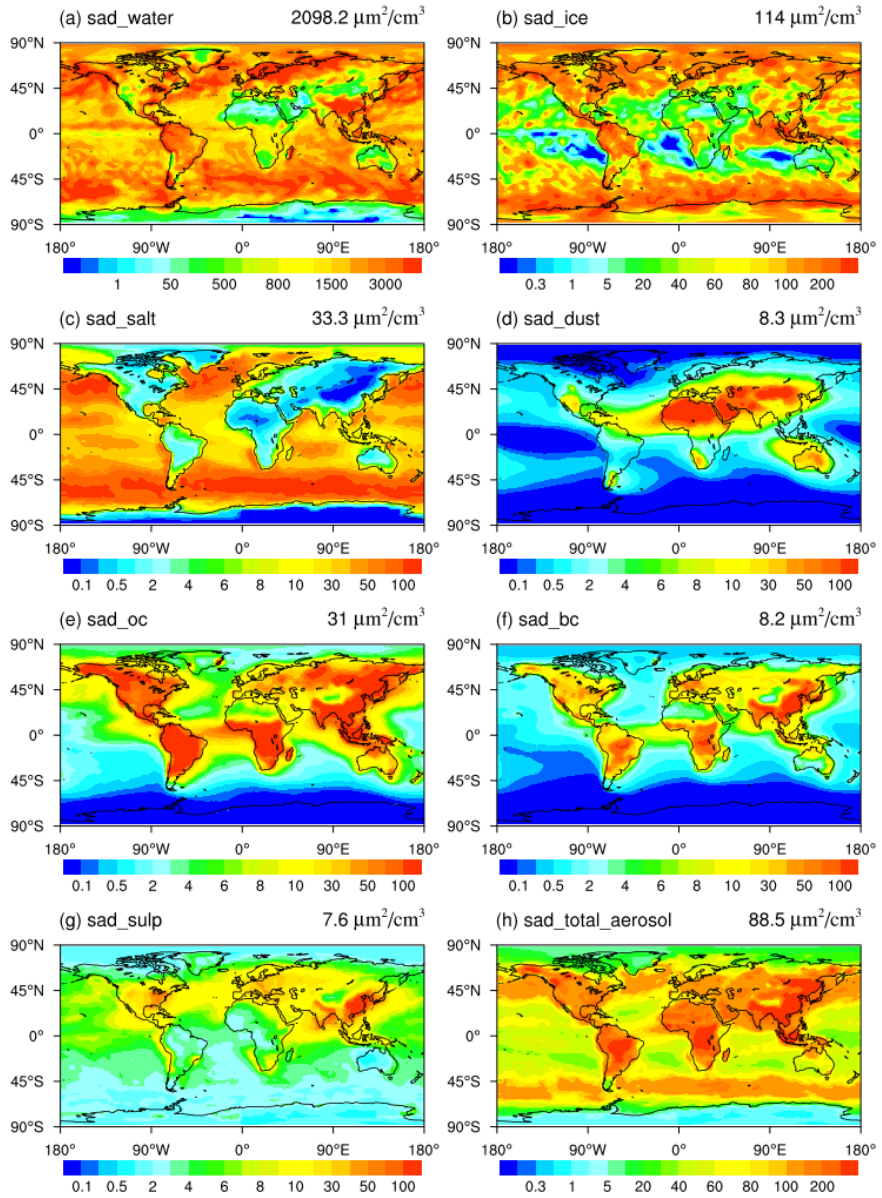

Figure S1. Global maps of the annual mean surface area density (SAD) of cloud water (a), cloud ice (b), sea salt (c), dust (d), organic carbon (e), black carbon (f), sulphate (g) and the total aerosol surface area density (h). All fields are derived from three-dimensional datasets, with cloud water and cloud ice from ECMWF meteorological fields and aerosols from CAMS climatology. Cloud SAD is averaged over the troposphere, while aerosol SAD is shown at the surface. Units are $\mu m^2 \cdot cm^{-3}$.

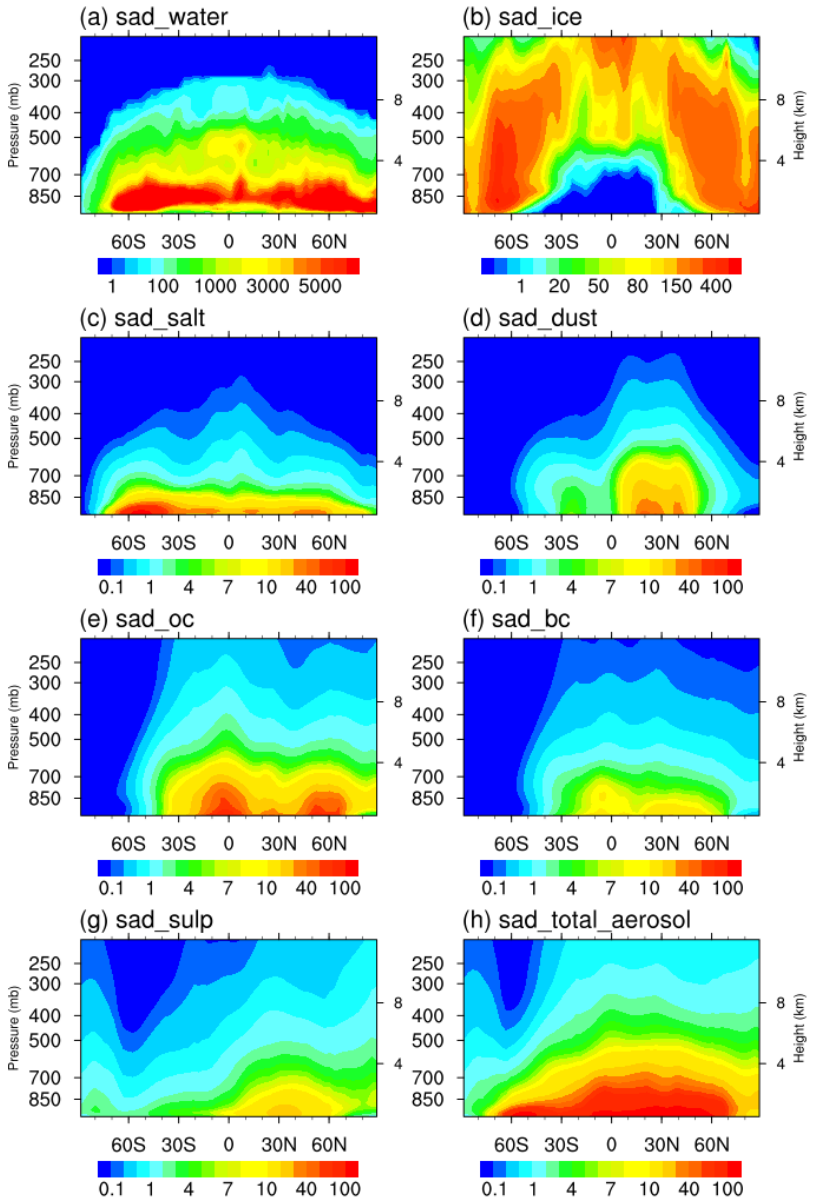

Figure S2. Annual Zonal-mean (latitude-pressure) cross sections of surface area density (SAD) for cloud water (a), cloud ice (b), sea salt (c), dust (d), organic carbon (e), black carbon (f), sulphate (g) and the total aerosol surface area density (h). Units are $\mu m^2 \cdot cm^{-3}$.

Table S4. The uptake coefficient (γ) in FRSGC/UCI CTM heterogeneous reactions.

surface	Uptake coefficient (γ)			
	N_2O_5+surface -> $2HONO_2$	HO_2+surface[6]	NO_2+surface->$0.5HONO_2$[3]	NO_3+surface->$HONO_2$[3]
Water	$2.7\times10^{-5}\exp(1800/T)$ [1]	0.1	10^{-8}	0.002
Ice	0.02[2,3]	0.1	0	0.001
Sea salt	0.005 (RH<62%) 0.03 (RH≥62%)[4,5]	0.1	10^{-8} (RH<40%) 10^{-4} (RH≥40%)	0.05 (RH<40%) 0.002 (RH≥40%)
Dust	0.02[2,3]	0.1	10^{-8}	0.01
Organic Carbon	RH×5.2*10^{-4} (RH<57%) 0.03 (RH≥57%)[4,5]	0.1	10^{-6}	0.005
Black Carbon	0.005[3,4]	0.1	10^{-4}	2.0×10^{-4} (RH<50%) 10^{-3} (RH≥50%)
Sulfate	$\gamma=\alpha\times10^{\beta}$ [4,5] $\alpha=2.79\times10^{-4}+1.3\times10^{-4}\times RH-3.43\times10^{-6}\times RH^2+7.52\times10^{-8}\times RH^3$	0.1	5.0×10^{-6}	0.001 (RH<40%) 0.002 (RH≥40%)

	$\beta=4\times10^{-2}\times(T-294)$ (T≥282K)
	β= -0.48 (T<282K)

Note: T is temperature (K), RH is relative humidity (%). 1. Ammann et al. (2013); 2. Crowley et al. (2010); 3. Holmes et al. (2019); 4. Evans and Jacob (2005); 5. Monks et al. (2017); 6. Ha et al. (2021).

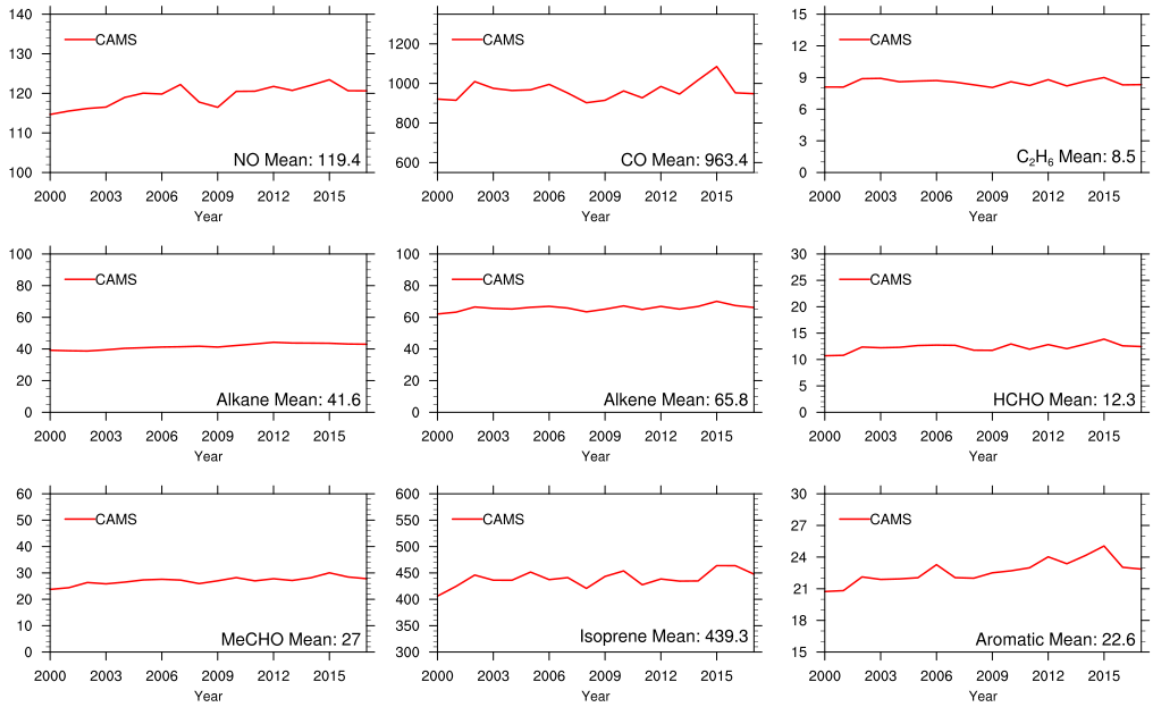

Figure S3. Global annual emissions from all sources (Tg·yr^{-1}) during 2000–2017, derived from multiple emission inventories: CAMS (including anthropogenic, aircraft, biogenic, and soil sources), GFED4s (fires), and POET (ocean). Detailed descriptions of these emission inventories are provided in Section 2.4 of the main text. The values in the bottom of each panel are the multiyear average.

Table S5. Global tropospheric O_3 burden (Tg) and budget terms (Tg·yr^{-1}) from previous model studies and this work.

Models	Prod	Loss	NetChem	Residual (STE)	DryDep	Burden	Lifetime (days)	Reference
33	3948±761	3745±554	245±346	636±273	902±255	307±38	21-25	Wild (2007)
17	4465±514	4114±409	396±247	529±105	949±222	314±33	22±2	Stevenson et al. (2006)
15	5110±606	4668±727	442±309	552±168	1003±200	344±39	22±2	Young et al. (2013)
4	3987-5315	3576-4476	411-869	28-481	791-892	310-357	23-29	Griffiths et al. (2021)
CESM FCSD	5038	4641	397	595	992	316/69	20	Hou et al. (2023)
FRSGC/UCI (T21L19)	4091	3854	237	519	757	283	23	Wild et al. (2004)
FRSGC/UCI (T42L57)								
CTL	5077±84	4379±86	698±16	316±21	1014±11	348±3	29±0.4	This study 2000-2017 mean
fixEmis	4952	4275	677	317	994	343	29	
noWVA	5149	4468	680	317	997	343	28	
noCloud	5152	4446	706	317	1024	353	29	
noAero	5229	4511	717	316	1034	351	28	
noHete	5314	4587	727	317	1044	356	28	
JPL	5374	4630	744	317	1061	363	29	

CTL	5231	4503	728	293	1021	351	28	This study 2016-2017
ALD-cesm	5262	4528	734	292	1026	352	28	
ALD-geoc	5275	4539	736	292	1028	353	28	

Note: Prod for chemical production, Loss for chemical loss, NetChem for net chemical production (Prod-Loss) and DryDep for dry deposition; Residual is the term balance by Residual=Loss-Prod+DryDep. The values following the ± in the CTL represent the standard deviation. Units of Prod, Loss, NetChem, Residual and DryDep are in $Tg(O_3)\cdot yr^{-1}$, Burden in $Tg(O_3)$, and Lifetime in days. The climatological pressure tropopause is used. The results of Griffiths et al. (2021) are the average of four models (UKESM1, CESM2-WACCM, GFDL-ESM4, MRI-ESM2-0), and the time is averaged from 1995 to 2004.

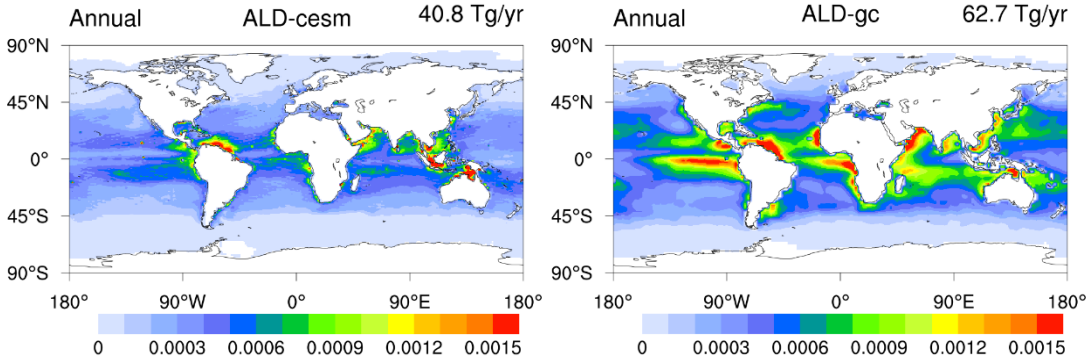

Figure S4 Simulated global distribution of CH3CHO ocean emissions (annual average) for ALD-cesm and ALD-gc runs.

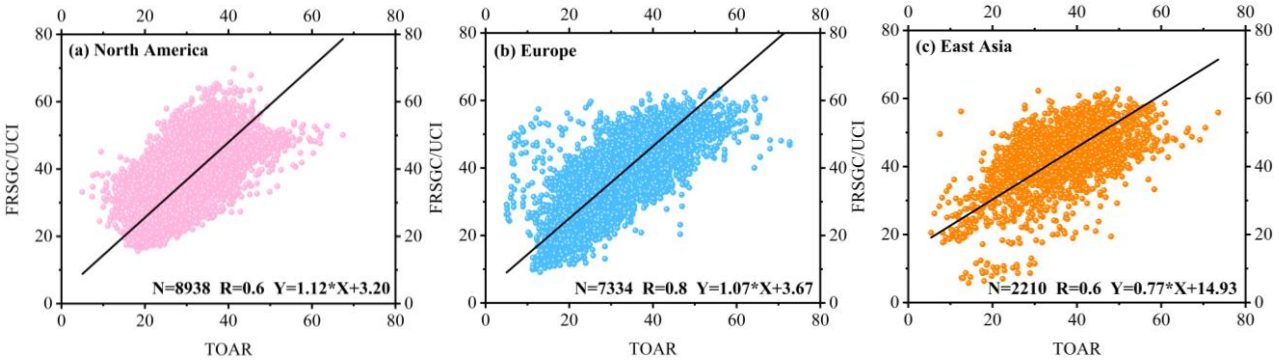

Figure S5. Scatter plots comparing monthly mean surface O_3 (ppbv) from the model control run with gridded observations from TOAR for three major regions: (a) North America, (b) Europe, and (c) East Asia during 2000–2014. Each point represents a monthly mean value for a grid cell within the corresponding region. The solid line indicates the linear regression fit, and number of data points (N), the correlation coefficient (R), and regression equation are shown in each panel.

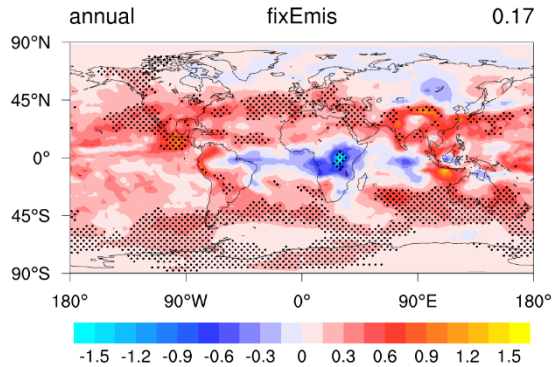

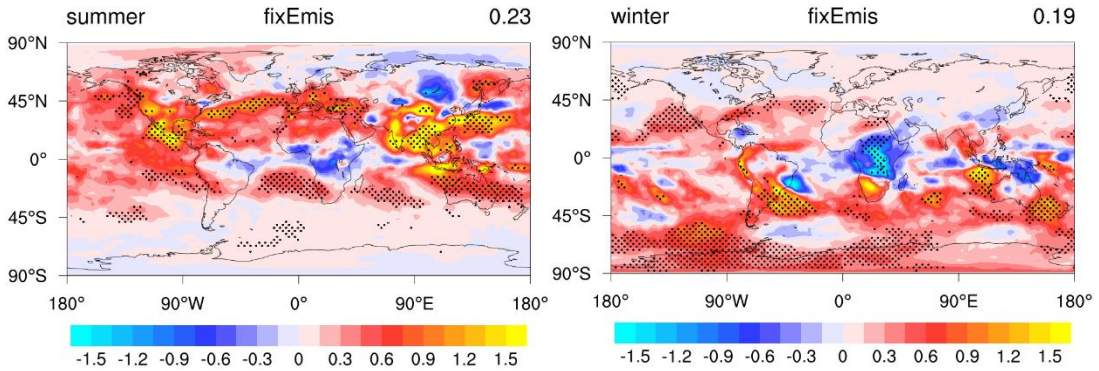

Figure S6. The trend of TCOH (10^{11} molec·cm^{-2}·yr^{-1}) in annual, winter and summer from 2000 to 2017. The troposphere was defined as the area below a climatological tropopause (p= 300-215(cos(lat))^2) (as discussed in Lawrence et al. (2001)). Trends are calculated as the same as Figure 1. Using the fixEmis experiment in Table 1.

References

Amedro, D., Bunkan, A. J. C., Berasategui, M., and Crowley, J. N.: Kinetics of the OH + NO2 reaction: rate coefficients (217–333 K, 16–1200 mbar) and fall-off parameters for N2 and O2 bath gases, Atmos. Chem. Phys., 19, 10643–10657, https://doi.org/10.5194/acp-19-10643-2019, 2019.

Ammann, M., Cox, R. A., Crowley, J. N., Jenkin, M. E., Mellouki, A., Rossi, M. J., Troe, J., and Wallington, T. J.: Evaluated kinetic and photochemical data for atmospheric chemistry: Volume VI – heterogeneous reactions with liquid substrates, Atmos. Chem. Phys., 13, 8045–8228, https://doi.org/10.5194/acp-13-8045-2013, 2013.

Atkinson, R., Baulch, D. L., Cox, R. A., Crowley, J. N., Hampson, R. F., Hynes, R. G., Jenkin, M. E., Rossi, M. J., and Troe, J.: Evaluated kinetic and photochemical data for atmospheric chemistry: Volume I - gas phase reactions of Ox, HOx, NOx and SOx species, Atmos. Chem. Phys., 4, 1461–1738, https://doi.org/10.5194/acp-4-1461-2004, 2004.

Atkinson, R., Baulch, D. L., Cox, R. A., Crowley, J. N., Hampson, R. F., Hynes, R. G., Jenkin, M. E., Rossi, M. J., Troe, J., and IUPAC Subcommittee: Evaluated kinetic and photochemical data for atmospheric chemistry: Volume II – gas phase reactions of organic species, Atmos. Chem. Phys., 6, 3625–4055, https://doi.org/10.5194/acp-6-3625-2006, 2006.

Burkholder, J. B., Sander, S. P., Abbatt, J., Barker, J. R., Cappa, C., Crounse, J. D., Dibble, T. S., Huie, R. E., Kolb, C. E., Kurylo, M. J., Orkin, V. L., Percival, C. J., Wilmouth, D. M., and Wine, P. H.: Chemical Kinetics and Photochemical Data for Use in Atmospheric Studies, Evaluation No. 19, JPL Publication 19-5, Jet Propulsion Laboratory, Pasadena, https://dataverse.jpl.nasa.gov/dataset.xhtml?persistentId=hdl:2014/49199&version=2.1, May 1, 2020.

Crowley, J. N., Ammann, M., Cox, R. A., Hynes, R. G., Jenkin, M. E., Mellouki, A., Rossi, M. J., Troe, J., and Wallington, T. J.: Evaluated kinetic and photochemical data for atmospheric chemistry: Volume V – heterogeneous reactions on solid substrates, Atmos. Chem. Phys., 10, 9059–9223, https://doi.org/10.5194/acp-10-9059-2010, 2010.

Evans, M. J., and Jacob, D. J.: Impact of new laboratory studies of N2O5 hydrolysis on global model budgets of tropospheric nitrogen oxides, ozone, and OH, Geophysical Research Letters, 32, L09813, https://doi.org/10.1029/2005GL022469, 2005.

Griffiths, P. T., Murray, L. T., Zeng, G., Shin, Y. M., Abraham, N. L., Archibald, A. T., Deushi, M., Emmons, L. K., Galbally, I. E., Hassler, B., Horowitz, L. W., Keeble, J., Liu, J., Moeini, O., Naik, V., O'Connor, F. M., Oshima, N., Tarasick, D., Tilmes, S., Turnock, S. T., Wild, O., Young, P. J., and Zanis, P.: Tropospheric ozone in CMIP6 simulations, Atmos. Chem. Phys., 21, 4187–4218, https://doi.org/10.5194/acp-21-4187-2021, 2021.

Ha, P. T. M., Matsuda, R., Kanaya, Y., Taketani, F., and Sudo, K.: Effects of heterogeneous reactions on tropospheric chemistry: a global simulation with the chemistry–climate model CHASER V4.0, Geosci. Model Dev., 14, 3813–3841, https://doi.org/10.5194/gmd-14-3813-2021, 2021.

Holmes, C. D., Bertram, T. H., Confer, K. L., Graham, K. A., Ronan, A. C., Wirks, C. K., & Shah, V.: The role of clouds in the tropospheric NOx cycle: A new modelling approach for cloud chemistry and its global implications, Geophys. Res. Lett., 46, 4980–4990. https://doi.org/10.1029/2019GL081990, 2019.

Hou, X., Wild, O., Zhu, B., and Lee, J.: Future tropospheric ozone budget and distribution over east Asia under a net-zero scenario, Atmos. Chem. Phys., 23, 15395–15411, https://doi.org/10.5194/acp-23-15395-2023, 2023.

Lawrence, M. G., Jöckel, P., and von Kuhlmann, R.: What does the global mean OH concentration tell us?, Atmos. Chem. Phys., 1, 37–49, https://doi.org/10.5194/acp-1-37-2001, 2001.

Monks, S. A., Arnold, S. R., Hollaway, M. J., Pope, R. J., Wilson, C., Feng, W., Emmerson, K. M., Kerridge, B. J., Latter, B. L., Miles, G. M., Siddans, R., and Chipperfield, M. P.: The TOMCAT global chemical transport model v1.6: description of chemical mechanism and model evaluation, Geosci. Model Dev., 10, 3025–3057, https://doi.org/10.5194/gmd-10-3025-2017, 2017.

Naik, V., Voulgarakis, A., Fiore, A. M., Horowitz, L. W., Lamarque, J.-F., Lin, M., Prather, M. J., Young, P. J., Bergmann, D., Cameron-Smith, P. J., Cionni, I., Collins, W. J., Dalsøren, S. B., Doherty, R., Eyring, V., Faluvegi, G., Folberth, G. A., Josse, B., Lee, Y. H., MacKenzie, I. A., Nagashima, T., van Noije, T. P. C., Plummer, D. A., Righi, M., Rumbold, S. T., Skeie, R., Shindell, D. T., Stevenson, D. S., Strode, S., Sudo, K., Szopa, S., and Zeng, G.: Preindustrial to present-day changes in tropospheric hydroxyl radical and methane lifetime from the Atmospheric Chemistry and Climate Model Intercomparison Project (ACCMIP), Atmos. Chem. Phys., 13, 5277–5298, https://doi.org/10.5194/acp-13-5277-2013, 2013.

Rolletter, M., Hofzumahaus, A., Novelli, A., Wahner, A., and Fuchs, H.: Kinetics of the reactions of OH with CO, NO, and NO2 and of HO2 with NO2 in air at 1 atm pressure, room temperature, and tropospheric water vapour concentrations, Atmos. Chem. Phys., 25, 3481–3502, https://doi.org/10.5194/acp-25-3481-2025, 2025.

Spivakovsky, C.M., Logan, J.A., Montzka, S.A., Balkanski, Y., Foreman-Fowler, M.S., Jones, D.B., Horowitz, L.W., Fusco, A.C., Brenninkmeijer, C.A., Prather, M.J., Wofsy, S.C., & McElroy, M.B.: Three-dimensional climatological distribution of tropospheric OH: Update and evaluation, J. Geophys. Res., 105, 8931-8980, 2000.

Stevenson, D. S., Dentener, F. J., Schultz, M. G., Ellingsen, K., van Noije, T. P. C., Wild, O., Zeng, G., Amann, M., Atherton, C. S., Bell, N., Bergmann, D. J., Bey, I., Butler, T., Cofala, J., Collins, W. J., Derwent, R. G., Doherty, R. M., Drevet, J., Eskes, H. J., Fiore, A. M., Gauss, M., Hauglustaine, D. A., Horowitz, L. W., Isaksen, I. S. A., Krol, M. C., Lamarque, J. F., Lawrence, M. G., Montanaro, V., Muller, J. F., Pitari, G., Prather, M. J., Pyle, J. A., Rast, S., Rodriguez, J. M., Sanderson, M. G., Savage, N. H., Shindell, D. T., Strahan, S. E., Sudo, K., and Szopa, S.: Multimodel ensemble simulations of present-day and near-future tropospheric ozone, J. Geophys. Res.-Atmos., 111, D08301, doi:10.1029/2005jd006338, 2006.

Wild, O.: Modelling the global tropospheric ozone budget: exploring the variability in current models, Atmos. Chem. Phys., 7, 2643–2660, https://doi.org/10.5194/acp-7-2643-2007, 2007.

Wild, O., Pochanart, P., and Akimoto, H.: Trans-Eurasian of ozone and its precursors, J. Geophys. Res., 109, D11302, doi:10.1029/2003JD004501, 2004.

Wild, O., Zhu, X., and Prather, M. J.: Fast-J: Accurate simulation of in- and below-cloud photolysis in tropospheric chemical models, J. Atmos. Chem., 37, 245–282, https://doi.org/10.1023/A:1006415919030, 2000.

Young, P. J., Archibald, A. T., Bowman, K. W., Lamarque, J.-F., Naik, V., Stevenson, D. S., Tilmes, S., Voulgarakis, A., Wild, O., Bergmann, D., Cameron-Smith, P., Cionni, I., Collins, W. J., Dalsøren, S. B., Doherty, R. M., Eyring, V., Faluvegi, G., Horowitz, L. W., Josse, B., Lee, Y. H., MacKenzie, I. A., Nagashima, T., Plummer, D. A., Righi, M., Rumbold, S. T., Skeie, R. B., Shindell, D. T., Strode, S. A., Sudo, K., Szopa, S., and Zeng, G.: Pre-industrial to end 21st century projections of tropospheric ozone from the Atmospheric Chemistry and Climate Model Intercomparison Project (ACCMIP), Atmos. Chem. Phys., 13, 2063–2090, https://doi.org/10.5194/acp-13-2063-2013, 2013.